Tacticity Effects on Polymer Blend Miscibility. 2. Rate of Phase Separation

G. Beaucage*,† and R. S. Stein

Department of Polymer Science and Engineering, University of Massachusetts, Amherst, Massachusetts 01003

Received May 5, 1992

ABSTRACT: Cloud-point curves of isotactic and atactic poly(vinyl methyl ether) (i- and a-PVME) blended with atactic polystyrene (PS) were analyzed using the Flory–Huggins–Staverman (F–H–S) approach in the *first paper*[1] *of this series*. A functional form for the composition-dependent interaction parameter, "*g*", in these two polymer blends was obtained. In this paper the "*g*" functions previously obtained are used to predict the rate of phase separation in terms of the apparent diffusion constant. The F–H–S analysis of cloud-point curves predicts a drastically slower rate of phase separation for i-PVME in blends with PS in comparison with a-PVME blends. The rate of phase separation is experimentally determined for these two polymer blends using light scattering. A comparison is made between the measured apparent diffusion constant and that predicted from simple cloud-point measurements using the F–H–S approach. The experimental kinetics data agree with the drastically slowed rate of phase separation predicted for the isotactic blend. A comparison of F–H–S results and the measured kinetics yields a translational diffusion constant which agrees with literature values. A brief discussion of a novel analysis of light scattering data from intermediate-stage phase separation is also presented. This analysis is based on a modified Cahn–Hilliard approach and uses the "*g*" functions obtained from cloud-point curves using the F–H–S approach.

Introduction

Equilibrium thermodynamics govern the direction in which nonequilibrium phase separation will tend in a binary blend. In a practical blend the domain sizes and final morphology will be governed by phase-separation thermodynamics coupled with the transport and interfacial properties of the blend components. It is convenient to divide phase-separation behavior in polymer blends of critical composition into three stages. The early stage of spinodal phase separation is to some degree of accuracy described by a balance of thermodynamic and transport properties using Cahn–Hilliard theory.[2,3] The intermediate stage of phase separation can be viewed as a process displaying spinodal-like behavior with a modified thermodynamic driving force based on a changing local composition. This has been a matter of recent investigation and will be discussed in the latter part of this paper. Late-stage phase separation is generally described by Ostwald ripening.[4,5] Late stages depend on surface tensions between components, the viscosity of components, and variety of other parameters such as stress fields in the material. The bulk of this paper will deal with the early stage in terms of Cahn–Hilliard theory.

In the first paper of this series[1] the Flory–Huggins–Staverman (F–H–S) equation was used to determine a functional form for the composition and temperature dependence of the interaction function, "*g*", in isotactic and atactic poly(vinyl methyl ether) (i- and a-PVME)/polystyrene (PS) blends based on cloud-point measurements. Using this approach the parameters a, b_0, b_1, and c (the latter being termed the Staverman parameter) are determined in the F–H–S equation.

$$g(\phi_2,T) = a + \frac{(b_0 + b_1/T)}{(1 - c\phi_2)} \tag{1}$$

The thermodynamic driving force for phase separation at early stages, $(g-g_s)/g_s$ (see the appendix), can be calculated, where g_s is the composition-dependent interaction parameter at the spinodal temperature. In this paper it will be shown that the $g(\phi,T)$ functions predict drastically slowed kinetics of phase separation for i-PVME/PS blends (in comparison with a-PVME/PS blends). Since the $g(\phi,T)$ functions are determined from cloud-point curves at the miscibility limit, we view the predictions for phase-separation kinetics well into the two-phase regime as a test of the usefulness of the F–H–S approach. Light scattering measurements will be used to determine the rate of phase separation in the isotactic and atactic PVME/PS blends. The results of kinetics measurements in the immiscible regime are compared with the predictions derived from cloud-point curves at the miscibility limit. A quantitative agreement will be demonstrated.

In addition, intermediate stages of phase separation will be briefly explored. Functional forms for the composition and temperature dependence of the thermodynamic driving force for phase separation are successfully used to describe intermediate stages using a variable local composition.

Cahn–Hilliard Theory

The linear Cahn–Hilliard theory[2,3] for the early stages of phase separation has been used to analyze light scattering data[6,7] from phase-separating polymer blends. During the initial stages of phase separation the intensity of light scattered at all angles is expected to increase exponentially,

$$I(q,t) = I(q,t=0)\,\exp(2R(q)t) \tag{2}$$

where $q = (4\pi/\lambda)\sin(\theta/2)$, t is the time of phase separation, and $R(q)$ is the amplification factor for phase separation or the growth rate for a size scale describe by $2\pi/q$. Cahn–Hilliard theory defines $R(q)$ for an incompressible blend as

$$R(q) = D_c q^2\left(-\left(\frac{\delta^2 f}{\delta {\phi_2}^2}\right) - 2\kappa q^2\right) \tag{3}$$

where D_c is the translational diffusion constant, f is the free energy density of the system at composition ϕ_2, and κ is the coefficient of the composition gradient.

† Supported in part by a grant from Polysar Inc. Present address: Sandia National Laboratories, Albuquerque, NM 87185.

0024-9297/93/2226-1609$04.00/0

Table I
Flory-Huggins-Staverman Analysis Parameters from Fits to the Cloud-Point Curves (Values Determined in the First Paper of This Series[1])

	a ($\times 10^3$)	b_0 ($\times 10^2$)	b_1	c
hetero	-1.43	1.36	-4.69	0.36[a]
iso	-0.57	1.77	-4.08	0.425
$\frac{\Delta\text{value}}{\text{avg value}}$	0.86	0.20	0.14	0.17

[a] From Bondi.[10]

For binary blends of linear polymers under the mean-field approximation, eq 3 has been given by (see refs 6 and 8)

$$R(q) = D_c q^2\left(\frac{(\chi - \chi_s)}{\chi_s} - \frac{R_0^2 q^2}{36}\right) \quad (4)$$

where χ is the Flory-Huggins interaction parameter, χ_s is the interaction parameter at the spinodal temperature, and R_0 is the unperturbed chain dimension. Equation 4 suggests plots of $R(q)/q^2$ versus q^2 in order to determine the apparent diffusion constant, D_{app},

$$D_{app} = D_c(T)\left(\frac{\chi - \chi_s}{\chi_s}\right) \quad (5)$$

and $(D_c R_0^2/36)$. As is indicated by eq 5, D_{app} is equal to zero at the spinodal temperature. The value of q for which $R(q) = 0$ is termed the critical q (q_c). Composition fluctuations with wavenumbers larger than this q_c value will not decompose into phase-separated structures. Equation 4 also predicts a balance between transport and thermodynamic effects which leads to a maximum in $R(q)$ at "q_m". "q_m" is related to "q_c" by

$$q_m^2 = q_c^2/2 \quad (6)$$

"q_m" is the q value at the intitial stages for the scattering "halo" from spinodal decomposition of blends discussed in a previous paper.[9]

For blends displaying a composition-dependent interaction parameter, $g(\phi)$, eq 4 can be approximated by

$$R(q) = D_c q^2\left(\frac{(g - g_s)}{g_s} - \frac{R_0^2 q^2}{36}\right) \quad (7)$$

and eq 5 by

$$D_{app} = D_c(T)\left(\frac{g - g_s}{g_s}\right) \quad (8)$$

as discussed in the appendix.

Predictions Concerning Kinetics of Phase Separation from F-H-S Analysis of Cloud-Point Curves

Using the values for a, b_0, b_1, and c (Table I) determined from cloud-point curves in the first paper of this series,[1] it is possible to predict g (composition-dependent χ-parameter) over a range of temperatures. One use for such predicted g values is in the estimation of the growth rate for phases in the immiscible regime using eqs 7 and 8. Since the behavior of g is predicted from data at the miscibility limit (for the case of cloud-point data), a successful prediction into the immiscible regime could be considered a test of the formalisms used in deriving the g function.

As discussed above, the thermodynamic driving force for phase separation in the immiscible regime can be approximated as (appendix)[6,8]

$$\frac{D_{app}}{D_c(T)} = \frac{(g - g_s)}{g_s}$$

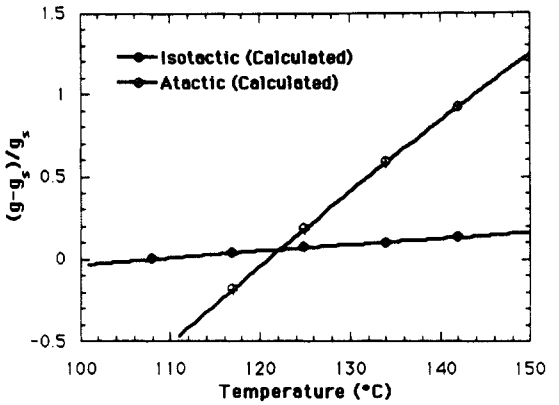

Figure 1. Predicted behavior for $(g - g_s)/g_s$ from the F-H-S analysis. This is the thermodynamic driving force for phase separation above the coexistence curve. Isotactic PVME shows lower miscibility and much slower kinetics above the miscibility limit $(g - g_s)/g_s = 0$.

We consider blends of critical composition (≈75% PVME by weight) so as to avoid the metastable binodal region) and predict the thermodynamic driving force for phase separation for the isotactic and atactic blends (Figure 1).

In this analysis g_s was calculated using the F-H-S parameters of Table I in eq 1 and the cloud-point temperature for a 75% PVME blend under the assumption that this is the critical composition and the critical temperature ($T_{cp,iso} \approx 109$ °C, $T_{cp,atactic} \approx 121$ °C). $(g - g_s)/g_s$ values calculated in this way are much smaller for the isotactic blend for similar quenches above the critical temperature. The rate of phase separation for the i-PVME blend is predicted to be drastically slower than the rate for the a-PVME/PS blend ($D_c(T)$ is expected to have very similar values for the different tacticities since they have essentially identical glass transition temperatures and similar molecular weights). The spinodal interaction parameter can also be calculated from the second derivative of the free energy which yields a comparable value for g_s. The experimentally measured critical point was used since it was felt that this was a more direct value.

Experimental Section

Isotactic PVME, i89 ($M_W = 89\,000$, $M_N = 49\,100$, $M_Z = 144\,900$), was prepared using cationic polymerization followed by solvent fractionation as previously described.[9] Atactic PVME, a99 ($M_W = 99\,000$, $M_N = 46\,500$, $M_Z = 151\,300$), was purchased from Scientific Polymer Products Inc. and fractionated.[9] The triad tacticities of the two polymers were determined using proton NMR (a99, 31% isotactic and 69% heterotactic; i89, 55% isotactic, 40% heterotactic, and 5% syndiotactic). The glass transition temperature for the two polymers was essentially identical, -29 °C, in accord with the findings of Karasz and MacKnight[11] for other monosubstituted vinyl polymers. Nominally monodisperse PS, $M_W/M_N = 1.03$, of molecular weight $M_W = 120\,000$ (Polymer Laboratories, Amherst, MA) was blended with each of the two PVME samples. Molecular weights of all polymers are reported as measured by GPC in terms of polystyrene standards. A Mark-Houwink analysis of the isotactic and atactic PVME indicated that this leads to errors in the molecular weight of less than 5%, which is within the accuracy of the measured values.

Blends of PVME/PS were cast from toluene solutions at 30 °C and allowed to air dry. The films were further dried in a vacuum oven at 70 °C for a week and finally in a vacuum oven at 100 °C for at least 6 h before scattering measurements were

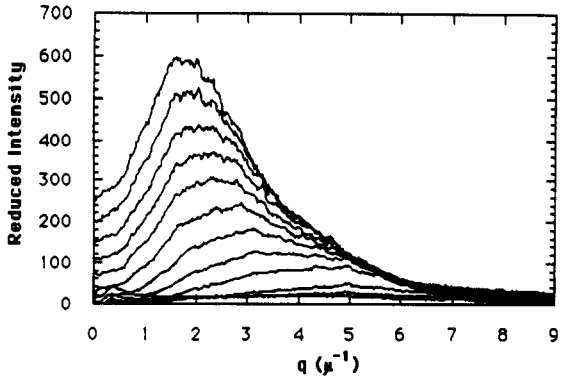

Figure 2. Series of light scattering measurements for isotactic PVME blended with PS (75% PVME) at 130 °C. (The critical temperature is 109 °C.) The patterns are separated by about 1 min and monotonically increase in intensity with time.

made. Kinetic measurements were made on thin films generally close to 10 μm thick held between two glass cover slips. These thin samples are necessary in order to reduce multiple scattering. A one-dimensional solid-state detector (OMA I made by Princeton Instruments) coupled with a PC was used to perform the kinetics studies. A screen was used to produce a real image of the scattering pattern, and a macrozoom lens was attached to the detector. The detector, lens, and screen were tilted at an angle of 30° from the main beam. The hot stage and sample were set at an angle of about 25° in order to circumvent internal reflection from the cover slip/air interface. Using this apparatus, angles from 0° to 75° could easily be observed. Adjustments for a smaller angular range could be made in minutes with this setup. The kinetics measurements reported in this paper were performed on 75% by weight PVME blends parepared as described above. This composition has been determined to be close to the critical composition for these blends; thus, only spinodal decomposition is expected in the early stages. (Off-critical compositions will phase separate via spinodal decomposition only in deep quenches).

Samples for the kinetics measurements were equilibrated at about 100 °C on a hot stage near the apparatus and quickly transferred to the apparatus which was at the experimental temperature. Due to the small mass of the cover slips and samples, thermal equilibrium was reached in much less than a minute as measured with a thermocouple attached to the cover slip.

Kinetics of Phase Separation

From the predictions of Figure 1 we can make three qualitative statements concerning the relative kinetics for phase separation in isotactic and atactic blends of PVME/PS. First, the driving force for phase separation is dramatically smaller for isotactic PVME in blends with PS in comparison with atactic PVME, second, the dependence of the growth rate on quench depth for i-PVME is very weak (the slope of $(g - g_s)/g_s$ in temperature is much smaller than the slope for atactic PVME), and finally the miscibility limit is lower for isotactic PVME blends (a direct result of the cloud-point measurement at T_c).

Figures 2 and 3 show a series of light scattering patterns (reduced intensity versus q) for isotactic and atactic PVME blended with polystyrene (75% by weight PVME). In both cases the intensity monotonically increases as a function of time, the curves being separated by about 1 min in both cases. The cloud points for the blends shown in Figures 2 and 3 occur at about 109 °C for the isotactic blend and at about 112 °C for the atactic blend. The patterns for Figure 2 (isotactic) were measured at 130 °C (a quench depth of 21 °C). Figure 3 was measured at 123 °C (a quench depth of 2 °C). Curves in both figures are separated by about 1 min. Since the kinetic data in Figures 2 and 3 show comparable rates of phase separation for drastically different quenches. They dramatically show a tacticity effect on the phase-separation kinetics. When

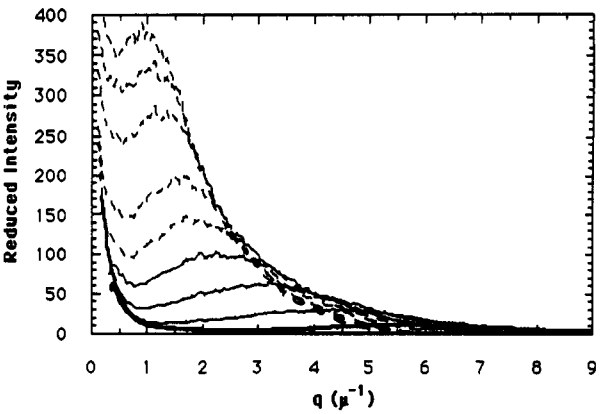

Figure 3. Series of light scattering measurements for atactic PVME blended with PS (75% PVME) at 123 °C. (The critical temperature is 121 °C.) The patterns are separated by about 1 min and monotonically increase in intensity with time.

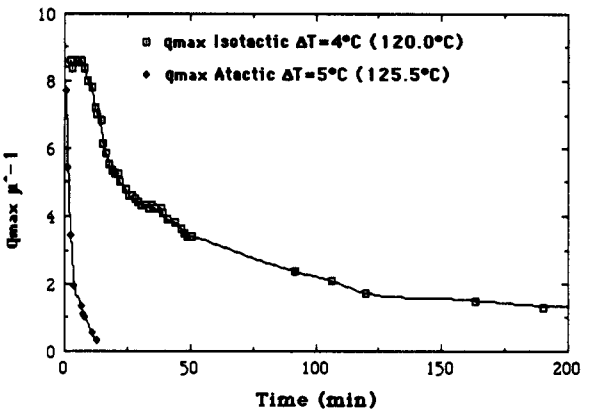

Figure 4. q_{max} versus time for isotactic and atactic PVME/PS blends of about 4 °C quench.

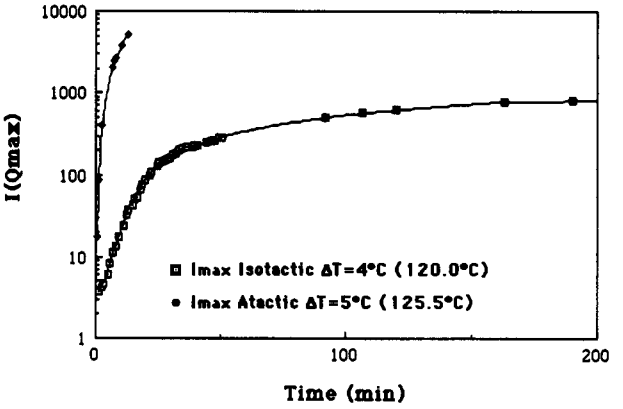

Figure 5. Dependence of the maximum in scattering intensity on time for isotactic and atactic PVME/PS blends.

comparisons are made between different quenches of the isotactic blends, only small changes in the rate of phase separation are observed. Thus, the small changes in phase separation rate with quench depth and the relatively slower rate of phase separation for the isotactic blends predicted by the F-H-S analysis are qualitatively confirmed.

Plots of the q value for the maximum in scattering intensity, q_{max}, versus time and the corresponding reduced intensity I_{max} versus time are given in Figures 4 and 5 for the isotactic and atactic blends at a quench depth of about 4 °C (120 and 126 °C, respectively). At this quench depth the isotactic material shows a region of constant q_{max} for about 10 min, followed by movement of q_{max} to smaller angles. The atactic material shows little if any region of constant q_{max}, and q_{max} rapidly decays to very low values. Thus, for similar quench depths the isotactic PVME/PS

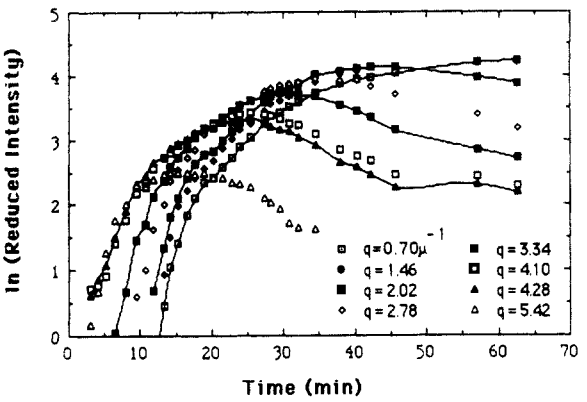

Figure 6. ln I versus time for a 16 °C quench of the isotactic blend as suggested by eq 1.

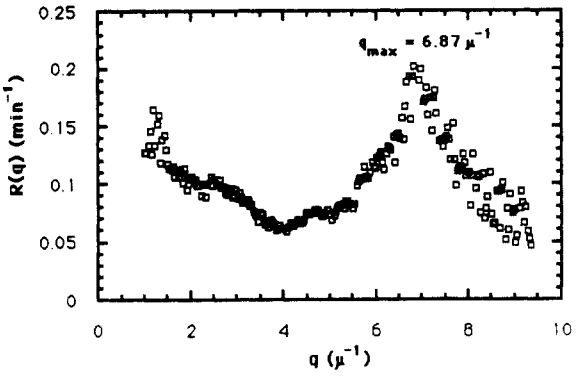

Figure 7. $R(q)$ vs q for the isotactic blend of Figure 5.

blend displays slowed kinetics when compared with atactic PVME/PS blends as predicted by the F–H–S analysis discussed in the companion paper.[1]

In Figure 5 the isotactic blend shows a large region of linear growth followed by a nonlinear region (intermediate stages of phase separation). The atactic material on the same time scale rapidly decomposes into a phase-separated material. Clearly, the growth in volume of the phases is much slower in the isotactic blend as predicted by the F–H–S analysis. In measurements at equal quench depths the kinetics are effected by the temperature dependence of D_c. This effect would increase the rate of phase separation (through $D_c(T)$) for the isotactic blend since it is measured at a higher temperature. The observed rate is, however, slower than that of the atactic PVME.

In Figure 6, ln I is plotted against time for a 16 °C quench of the isotactic blend, as suggested by eq 2. A series of q values are plotted.

At early stages ($t < 10$ min) a linear regime is observed for most of the q range. This corresponds to the early stages of phase separation for the isotactic blend. Deviation from linear Cahn–Hilliard behavior occurs at later times. The slopes of the linear region of Figure 6 are plotted versus q in Figure 7. A maximum in $R(q)$ occurs as indicated by Cahn–Hilliard theroy.

As noted above, eq 4 suggests plots of $R(q)/q^2$ versus q^2. Figure 8 shows such a plot for the data of Figures 6 and 7. A linear region is observed, and a value for the apparent diffusion constant of 7.6×10^{-3} $\mu m^2/s$ is obtained. For this case $q_c = 15$ μm^{-1} and a value of about $q_m = 10$ μm^{-1} is calculated from eq 6. This value is higher than the value indicated in Figure 7 (about 7 μm^{-1}). This may be accounted for by the distance of extrapolation from the measured values used in determining q_c (an order of magnitude) in the analysis of $R(q)/q^2$ versus q^2 plots.

Values for D_{app} versus temperature are plotted in Figure 9. An extrapolation to $D_{app} = 0$ is made in order to

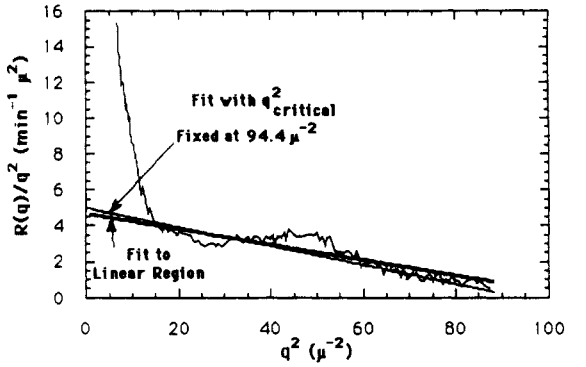

Figure 8. $R(q)/q^2$ versus q^2 for the isotactic blends of Figures 5 and 6.

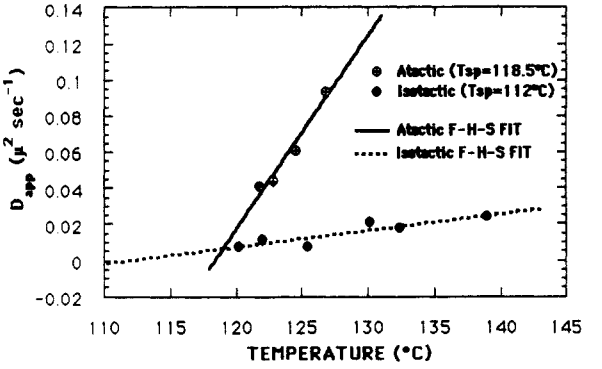

Figure 9. D_{app} versus quench temperature for 75 wt % isotactic and heterotactic PVME/PS blends for extrapolation to the spinodal point at $D_{app} = 0$. Lines are F–H–S fits using $(-K_cT)((g - g_s)/g_s)$ (with K_c as the only fit parameter) for the isotactic and atactic blends.

Table II
Spinodal Temperatures for Isotactic and Heterotactic PVME/PS Blends of 75 wt % PVME As Measured by D_{app} Extrapolation, Quench Measurements for Thin Films, and Cloud-Point Measurements for Thick Films

	isotactic blend	atactic blend
T_s (D_{app}), °C	113	119
T_{min} (thin films), °C	115	121
T_{cp} (thick films), °C	109	121

determine the spinodal temperature (eq 5) whose values are given as T_s in Table II. Three spinodal temperatures are indicated in Table II for the 75% PVME blends. Values obtained by the above extrapolation differed by about 2 °C from those measured using the cloud-point technique. T_{min} (thin films) is the minimum temperature at which phase separation could be induced by the quenching technique used in the kinetics measurements. The difference between the latter and the cloud-point measurement may be due to the difference in film thickness, indicated in the Experimental Section,[1,5,9] as has been noted by Cohen and Reich.[12] The small driving force for phase separation in the isotactic blends discussed above may be shifted by surface effects to a larger extent in the isotactic blends, leading to a larger discrepancy in the T_{min} and T_{cp} values in Table II.

Correlation between Flory–Huggins–Staverman Analysis and Kinetics Measurements

In the first paper of this series[1] F–H–S analysis was used to determine a functional form for the composition- and temperature-dependent interaction parameter, "g", from cloud-point measurements. These functional forms for "g" were used to predict the thermodynamic driving force for phase separation in the immiscible regime, $(g - g_s)/g_s$.

From the discussion given above there is qualitative agreement between the predictions of the F-H-S analysis[1] and the measured kinetics data (Figures 1 and 9). In Figure 9, a fit of the F-H-S functional form for $(g - g_s)/g_s$ has been applied to the measured D_{app} data. It is assumed that the translational diffusion constant has a linear temperature dependence in the 20 °C range studied, such that

$$D_{app} = D_c(T)\frac{(g - g_s)}{g_s} = K_c T\frac{(g - g_s)}{g_s} \quad (9)$$

The F-H-S equations for "g" are used to generate $(g - g_s)/g_s$, and K_c is used to fit the kinetics data. It is expected that tacticity would have little effect on the translational diffusion constant $D_c(T)$ since the two PVME's have identical glass transition temperatures and similar molecular weights. The values for $D_c(125\ °C)$, i.e., K_cT, obtained from the fit of Figure 9 are

$$D_{c,iso}(125\ °C) = -0.22\ \mu m^2/s$$

$$D_{c,atactic}(125\ °C) = -0.24\ \mu m^2/s$$

These values are close to other experimentally determined values such as those of Nishi, Wang, and Kwei[13] for the PS/PVME blend (determined using NMR, $D_c \approx -0.28$). The agreement between the two D_c values, and the agreement with literature values, supports the F-H-S analysis of the CPC reported in the companion paper.[1] Thus, we have quantitatively shown that the F-H-S analysis of cloud-point curves at the miscibility limit is useful in predicting phase-separation kinetics data in the immiscible regime for early stages of phase separation. In the next section F-H-S functional forms for "g" will be used to perform a preliminary analysis of intermediate-stage phase separation (i.e., the nonlinear regime of Figures 5 and 6).

Intermediate Stages of Phase Separation

The Cahn-Hilliard analysis (presented in the previous sections) was based on the initial stages of phase separation in which linear regions of ln I versus time plots are observed. This regime is described to some degree of satisfaction by linear Cahn-Hilliard theory. As can be seen from Figure 6 this regime (about 15 min in Figure 6) accounts for a very small portion of the data, and for larger quenches in blends with sizable values of D_{app} this region may not be observed at all. Many polymer blend systems have been reported in the literature for which a linear regime cannot be measured,[14] and generally a linear regime is not observed for metalurgical systems. Therefore, it is desirable to understand, at least in an empirical manner, the rich data which follows the initial linear region. It should be noted that the behavior which is observed in Figure 6 is fairly universal, occurring over the quench depth spectrum for both isotactic and atactic PVME of critical composition as well as for other blend systems reported in the literature.[6,14] A discussion of a novel approach to the analysis of intermediate-stage phase separation is presented below in which the variation of $(g - g_s)/g_s$ with composition (determined using the F-H-S parameters) is used to fit light scattering data from intermediate stages of phase separation at a single bulk composition. A similar approach was suggested by Langer[18] with regard to metallic alloys which show similar behavior (Figure 2, ref 18). A brief discussion of preliminary results will be presented. A full presentation of the results of this analysis as applied to the isotactic/atactic PVME/PS blends and other polymer blends will be presented in the future.

For a molecularly miscible binary blend the bulk composition describes the composition at all size scales of interest. Similarly, at the earliest stages of phase separation for a blend of critical composition the bulk composition can be used to ascertain the thermodynamic driving force for phase separation. Immediately following a quench into a two-phase regime, the bulk composition no longer describes the blend at certain size scales. As phase separation proceeds the size scale of the coexisting phases grows, resulting in a discrepancy between the bulk composition at larger and larger size scales. Thus, the phase-separation process involves two coexisting processes. In a critical composition binary blend of A and B for instance, component A is excluded from a phase predominantly composed of B and component B is excluded from a phase predominantly composed of A. Each of these phase-separation processes might be expected to be governed by a balance of thermodynamics and transport properties as described by Cahn-Hilliard theory. In this case the thermodynamic driving force is composed by a weighted sum of two terms, one describing each of these processes. Since the composition is shifted toward a more miscible regime as one leaves the critical composition, the average thermodynamic driving force for phase separation is diminished. (Reference should be made to Langer,[18] who discusses fine-grained and coarse-grained compositions in metallic alloys.)

For the case of a binary polymer blend of critical composition the composition dependence of the miscibility limit is generally flat in the immediate vicinity of the critical point. Thus, one would expect only small shifts in the thermodynamic driving force with composition changes at the initial stages. As phase separation proceeds, changes in the average depth of quench caused by shifts in composition of the coexisting phases reduce the thermodynamic driving force. This approach when coupled with Cahn-Hilliard theory predicts a collapsing halo in the light scattering pattern as is commonly observed. The collapsing halo is predicted directly from eqs 4 or 8 since, as $(\chi - \chi_s)/\chi_s$ or $(g - g_s)/g_s$ becomes smaller with a shift in composition, the maximum in $R(q)$ generated by $q^2((g - g_s)/g_s - R_0^2q^2/36)$ becomes smaller for a fixed R_0^2. Using this approach, a functional form for $g(T,\phi)$ is a prerequisite for further analysis of intermediate-stage phase separation. The F-H-S functional form will be used in this regard.

Recently,[15] Hashimoto and co-workers have observed that the early stages of spinodal phase separation in polymer blends give way to an intermediate stage of pseudospinodal phase separation characterized by a self-similar growth of composition fluctuations. That is, the size scale of the fluctuations grow while the structure remains similar to that of the early stages of spinodal decomposition, albeit on a larger size scale (Figure 11, top figures). This may be an indication that processes related to spinodal decomposition are important beyond the linear Cahn-Hilliard regime.

As shown schematically in Figure 10 the linear theory assumes that $(\chi - \chi_s)/\chi_s$ or $(g - g_s)/g_s$ is constant for a fixed temperature of quench in the equation

$$R(q) = D_c q^2\left(\frac{(g - g_s)}{g_s} - \frac{R_0^2q^2}{36}\right) \quad (7)$$

Since $(g - g_s)/g_s$ (g is used for a composition-dependent χ) depends on composition, the linear theory effectively assumes that composition is constant throughout the

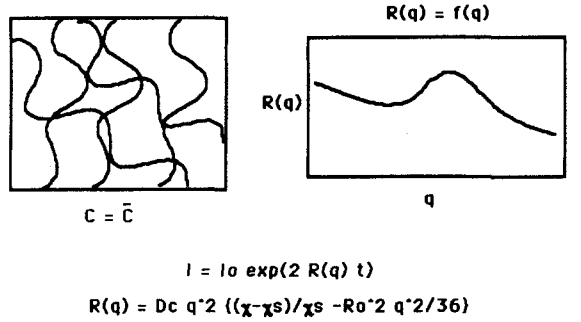

Figure 10. Schematic of linear Cahn–Hilliard theory. Left: schematic structure for spinodal decomposition (dark lines indicate regions of composition fluctuations). Right: dependence of $R(q)$ on q.

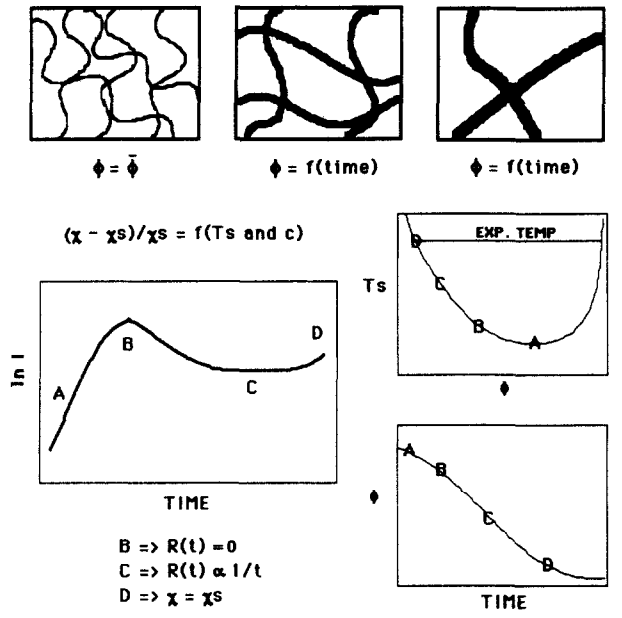

Figure 11. Self-similarity in intermediate stages on polymer phase separation. (Dark lines in the top figures indicate, schematically, regions of composition fluctuations. Magnification remains constant in the top three figures.)

phase-separation process. Experimentally, this assumption appears to be valid over a limited time range due to the flatness of the spinodal curve near the critical point (Figure 11, points marked "A") and due to the small local change in composition of the phase-separating species at the initial stages of phase separation.

Initially a decreasing $(g - g_s)/g_s$ in eq 4 yields a smaller value for $R(q)$ and consequently a decreasing slope of ln $I = \ln I_0 + 2R(q)\,t$ (eq 2). At some point $(\chi - \chi_s)/\chi_s$ becomes equal to $(R_0^2q^2)/36$ (eq 4) and the slope of ln(I) versus time (eq 2) goes to zero (B in Figure 11). Beyond this time in the phase separation, the slope $(2R(q))$ becomes negative (since $(R_0^2q^2)/36$ is larger than $(g - g_s)/g_s$). This is observed in the data (Figure 6). As time progresses further (C in Figure 11), composition becomes approximately linear in time in a region of composition for which time the spinodal temperature is linear in composition; thus, $(g - g_s)/g_s$, which depends roughly on the inverse of the spinodal temperature for a constant quench, becomes linear in 1/time and ln I $(=\ln I_0 + 2R(q)\,t)$ becomes independent of time. At later stages one would predict a linear decrease of intensity with time as $(g - g_s)/g_s$ goes to zero. Actually, a slight increase in intensity is observed at very long time scales in the blends studied here (D in Figure 11), indicating that the pseudospinodal model is no longer appropriate.

The functional form for "g" obtained using the F–H–S approach was used to estimate a decreasing $(g - g_s)/g_s$ with

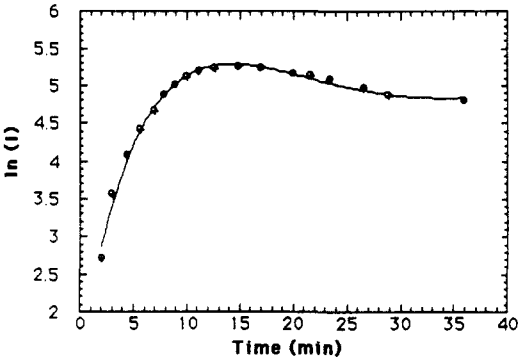

Figure 12. Typical fit of the scattering data using the pseudospinodal approach and the F–H–S equation for $(g - g_s)/g_s$ (eq 5.24). (123.5 °C, heterotactic PVME/PS, q = 1.84 μm^{-1}.)

time of quench. In order to simplify the analysis, only one of the two coexisting phase compositions was used to generate $(g - g_s)/g_s$. This is the equivalent of assuming a symmetric phase diagram about $\phi_{critical}$. "g" values from the polystyrene-rich phase were used in the analysis. Figure 12 is a typical fit of the data using this approach and the F–H–S equation for $(g - g_s)/g_s$ (eq 1). An exponential decrement in composition (ϕ versus time in Figure 11) was used to model the behavior shown schematically in Figure 11, yielding two unknown fitting parameters.. These parameters, however, can be determined from the data if it is assumed that the composition change with time is not dependent on the size scale of measurement (i.e., the q value) within the range of q values measured. (In this case the previous assumption yields 500 plots (for a 500-channel detector), similar to Figure 12, for each quench. In each of these plots these two parameters must remain constant.) The spinodal temperatures and the a, b_0, b_1, and c values ascertained in the F–H–S analysis were used to generate $(g - g_s)/g_s$ and $R(q)$ data. From preliminary results using this approach, values of $R(q)$ have been determined for isotactic PVME/PS blends which show a significant linear Cahn–Hilliard regime. $R(q)_{linear}$ values generally are close to the $R(q)$ values determined using this technique. Values of R_0 (the unperturbed radius of gyration for an average polymer chain in the blend) may be obtained in this way (one of the two fitting parameters). Generally the radius of gyration was in the 100-Å range which would agree with an average θ chain of the PVME/PS polymers.

This approach to analyzing the scattering data yield fits to the data over a wide range of q and time. Although not used in the present paper due to time constraints (each quench generated 500 I versus q data files each with time dependencies similar to Figure 11), it is believed to be a very promising approach which can result in a Cahn–Hilliard type analysis of scattering data on systems which show a very small (or no) linear regime in the ln I versus time data. Simplified functional forms for $g(T,\phi)$ are adequate for this analysis. For the quenches examined, preliminary values for D_{app} did not appear to significantly vary from the linear Cahn–Hilliard values for quenches in which the linear regime was well-defined. The use of a much broader range of q values and the loss of the linear assumption are hoped to yield more accurate fits and values for D_{app}. This may be particularly useful in blends which show only a limited linear Cahn–Hilliard regime. It would appear that this approach to intermediate stages of phase separation, with minor modifications, is applicable to nonmacromolecular blends. A more detailed presentation of the results of this analysis in the isotactic/atactic PVME/

PS blends and application to other polymer blends will be presented in the future.

Conclusions

The Flory–Huggins–Staverman theory using cloud-point data at the miscibility limit predicts drastically slowed phase-separation kinetics in the immiscible regime for the isotactic PVME blends with PS. Quantitatively, measurements of the phase-separation kinetics surprisingly support the prediction of the F–H–S analysis. As a test of this prediction the translational diffusion constants, D_c, of the two tacticities of PVME were calculated from fits of the apparent diffusion constant versus the quench depth. The value of D_c calculated in this way for isotactic and atactic PVME/PS blends was very similar and agreed with literature values obtained using an unrelated technique. (It is expected that these two values should agree for different tacticity monosubstituted vinyl polymers of similar molecular weight which do not show a shift in T_g.) Thus, a quantitative assessment of the agreement between the theoretical prediction and the measured kinetics was upheld.

An analysis of intermediate stages of phase separation taking advantage of the F–H–S predicted dependencies of the interaction parameter on composition and temperature and using a modified Cahn–Hilliard approach was presented. Scattering data over a wide range of q and time (well beyond the linear regime) can be fit using this approach. Preliminary results qualitatively agree with the results of a linear Cahn–Hilliard analysis. A full presentation of the application of this technique to the PVME/PS blends and other blend systems will be presented in the future. This analysis technique may be very useful for blends which show only a limited linear Cahn–Hilliard regime. The modified Cahn–Hilliard approach appears to be applicable to nonmacromolecular blends.

Appendix: Development of Equation 8

Derivations concerning nonequilibrium thermodynamics of polymer blends in the immiscible regime using the Flory–Huggins theory were first presented by Van Aartsen.[16] Van Aartsen developed an expression for the phase size of maximum growth rate during the early stages of spinodal decomposition. de Gennes[8] and Pincus[17] developed an expression describing the growth rate $R(q)$ using Flory–Huggins theory. Reference should also be made to the work of Langer[18] in metal alloys which discusses the issue of coarse-grain composition in a phase-separating system and his general work on first-order phase transitions which he has recently reviewed.[19] The derivation of eq 8 follows the development of de Gennes[8] and Hashimoto.[6]

The free enthalpy in the spinodal regime has been described by extending the Flory–Huggins equation to include a term describing spatial variations in composition. Similarly, for a composition-dependent interaction parameter,[1] g, and ignoring polydispersity, we have

$$\frac{\Delta G'}{NRT} = \frac{\phi_1}{m_1}\ln\phi_1 + \frac{\phi_2}{m_2}\ln\phi_2 + g\phi_1\phi_2 + \frac{a^2}{36\phi_1\phi_2}(\nabla\phi_1)^2 \quad \text{(A1)}$$

where "a" is the Kuhn statistical segment length, ϕ_i is the volume fraction of component i, m_i is the number of occupied lattice sites for macromolecule i, and N is the total number of lattice sites in moles.

The chemical potential difference between the two components of an early-stage nonhomogeneous binary system under the condition that the coarse-grain composition can be represented by a single composition is given by $[\Delta\mu_1'/\mu_1RT - \Delta\mu_2'/\mu_2RT] = \delta(\Delta G'/NRT)/\delta\phi_1$ (where $\Delta\mu_1'/\mu_1RT$ and $\Delta\mu_2'/\mu_2RT$ are analogous to eq 10 and 11 of the first paper in this series[1] with the addition of a gradient energy term and $\Delta G'/NRT$ is given above). The chemical potential difference is given by

$$\frac{\delta(\Delta G'/NRT)}{\delta\phi_1} = \frac{\ln\phi_1}{m_1} + \frac{1}{m_1} - \frac{\ln\phi_2}{m_2} - \frac{1}{m_2} + (1-2\phi_1)g + \phi_1\phi_2\frac{\delta g}{\delta\phi_1} - \frac{a^2}{36\phi_1\phi_2}(\nabla\phi_1)^2 \quad \text{(A2)}$$

The continuity equation

$$\frac{\delta\phi_1}{\delta t} + \operatorname{div} J = 0 \quad \text{(A3)}$$

is used to relate the chemical potential difference to the growth rate of composition fluctuations through the relation

$$J = -\Lambda\nabla\left[\frac{\Delta\mu_1'}{\mu_1RT} - \frac{\Delta\mu_2'}{\mu_2RT}\right] \quad \text{(A4)}$$

where Λ is an Onsager coefficient and J is the local flux of species 1.

Equations A2 and A4 are used to derive J (eq 3.4 of ref 8)

$$J = -\Lambda\left\{\left[\frac{1}{m_1\phi_1} + \frac{1}{m_2\phi_2} - 2g + (1-2\phi_1)\frac{\delta g}{\delta\phi_1} + \phi_1\phi_2\frac{\delta^2 g}{\delta\phi_1^2}\right]\nabla(\delta\phi_1) - \frac{a^2}{36\phi_1\phi_2}\nabla^3(\delta\phi_1)\right\} \quad \text{(A5)}$$

Using this expression in eq A3 and taking the Fourier transform using the derivative rule, we have

$$\frac{\delta(\delta\phi_{1q})}{\delta t} = (\delta\phi_{1q})\Lambda\left\{\left[\frac{1}{m_1\phi_1} + \frac{1}{m_2\phi_2} - 2g + (1-2\phi_1)\frac{\delta g}{\delta\phi_1} + \phi_1\phi_2\frac{\delta^2 g}{\delta\phi_1^2}\right]q^2 - \frac{a^2}{36\phi_1\phi_2}q^4\right\} \quad \text{(A6)}$$

The growth rate in the spinodal regime is given by

$$R(q) = -\frac{1}{\tau_q} = \frac{1}{\delta\phi_q}\frac{\delta(\delta\phi_q)}{\delta t} = -q^2\Lambda\left[\frac{1}{m_1\phi_1} + \frac{1}{m_2\phi_2} - 2g + (1-2\phi_1)\frac{\delta g}{\delta\phi_1} + \phi_1\phi_2\frac{\delta^2 g}{\delta\phi_1^2} + \frac{a^2}{36\phi_1\phi_2}q^2\right] \quad \text{(A7)}$$

The interaction parameter at the spinodal point is defined by $\delta^2(G/NRT)/\delta\phi_1^2 = 0$ which yields

$$2g_s = \left[\frac{1}{m_1\phi_1} + \frac{1}{m_2\phi_2} + (1-2\phi_1)\frac{\delta g}{\delta\phi_1} + \phi_1\phi_2\frac{\delta^2 g}{\delta\phi_1^2}\right] \quad \text{(A8)}$$

Thus, eq A7 can be written as

$$R(q) = q^2\Lambda(q)\left((2g - 2g_s) - \frac{a^2q^2}{36\phi_1\phi_2}\right) \quad \text{(A9)}$$

Under the assumption that the entanglement properties and friction coefficients are the same for the two "neat" components and for the components in a blend (i.e., $g = 0$ but $\delta g/\delta\phi_1$ and $\delta^2 g/\delta\phi_1^2$ are not necessarily zero), the Onsager coefficient at the small q limit (long diffusion

distances) has been given as[6(eq 2.7), 8(appendix A), 20]

$$\Lambda \approx \left[\frac{D_c}{\frac{\delta^2(G/NRT)}{\delta\phi_1^2}}\right]_{g=0} = \frac{D_c}{2g_s} \qquad \text{(A10)}$$

The dependence of g on composition might be due to structural changes in the polymers brought on by thermodynamic interactions. This has been discussed in the first paper of this series in terms of the degree of ordering of the isotactic PVME in the blend versus neat isotactic PVME (see F-H-S Cloud-Point Analysis in ref 1). Structural changes in the polymers clearly can be expected to have an effect on the transport properties of the materials. The "neat" components referred to above may therefore be hypothetical pure components which have identical structure to the blend components. In this way a composition dependence to the Onsager coefficient can be introduced while retaining some independence of transport from thermodynamic properties. A composition dependence to the radius of gyration is also expected.

Combining eqs A9 and A10, we have

$$R(q) = q^2 D_c\left(\frac{(g-g_s)}{g_s} - \frac{R_0^2 q^2}{36(2g_s)N\phi_1\phi_2}\right) \qquad \text{(A11)}$$

where $R_0^2 = Na^2$ is the average radius of gyration. We can further identify $(2N\phi_1\phi_2)^{-1}$ with the classic Flory–Huggins interaction parameter at the critical point in the absence of a composition dependence to the interaction parameter χ_c^*, yielding

$$R(q) = q^2 D_c\left(\frac{(g-g_s)}{g_s} - \frac{R_0^2 q^2}{36}\left(\frac{\chi_c^*}{g_s}\right)\right) = q^2 D_c\left(\frac{(g-g_s)}{g_s} - \frac{R^*{}_0^2 q^2}{36}\right) \qquad \text{(A12)}$$

where $R^*{}_0^2 = R_0^2(\chi^*{}_c/g_s)$ is an average radius of gyration modified for an interaction parameter which displays a composition dependence. $R^*{}_0^2$ displays a composition dependence since (χ_c^*/g_s) dispays a composition dependence.

In eq A12, an extrapolation of $R(q)/q^2$ to $q = 0$ yields

$$D_c(T)\frac{(g(\phi,T) - g_s(\phi))}{g_s(\phi)} = D_{app}(\phi,T) \qquad \text{(A13)}$$

where D_{app} is the observed apparent diffusion constant and $D_c(T)$ is a translational diffusion constant as defined by reptation theory (the implied dependencies have been made explicit).

References and Notes

(1) Part I of this series: Beaucage, G.; Stein, R. S.; Koningsveld, R. *Macromolecules*, previous paper in this issue.
(2) Cahn, J. W. *J. Chem. Phys.* **1965**, *42*, 93. Cahn, J. W.; Hilliard, J. E. *J. Chem. Phys.* **1959**, *28*, 258.
(3) Cook, H. E. *Acta Metall.* **1970**, *18*, 297.
(4) Olabisi, O.; Robeson, L. M.; Shaw, M. T. *Polymer–Polymer Miscibility*; Academic Press: New York, 1979.
(5) Wu, S. *Polymer Interface and Adhesion*; Marcel Dekker, Inc.: New York, 1982.
(6) Hashimoto, T.; Kumaki, J.; Kawai, H. *Macromolecules* **1983**, *16* (4), 641.
(7) Shibayama, M.; Yang, H.; Stein, R. S.; Han, C. C. *Macromolecules* **1985**, *18*, 2179.
(8) de Gennes, P.-G. *J. Chem. Phys.* **1980**, *27* (9), 4756.
(9) Beaucage, G.; Stein, R. S.; Hashimoto, T.; Hasegawa, H. *Macromolecules* **1991**, *24*, 3443–3448.
(10) Staverman, A. J. *Recl. Trav. Chim. Pays-Bas* **1937**, *56*, 885. Bondi, A. *J. Phys. Chem.* **1964**, *68*, 441.
(11) Karasz, F. E.; MacKnight, W. J. *Macromolecules* **1968**, *1* (6), 537.
(12) Reich, S.; Cohen, Y. *J. Polym. Sci., Polym. Phys. Ed.* **1981**, *19* (8), 1255.
(13) Nishi, T.; Wang, T. T.; Kwei, T. K. *Macromolecules* **1975**, *8*, 227.
(14) For example: Kyu, T.; Saldanha, J. M. Polycarbonate/PMMA Blends. *Macromolecules* **1988**, *21*, 1021.
(15) Hashimoto, T., personal communication.
(16) Van Aartsen, J. J. *Eur. Polym. J.* **1970**, *6*, 919–924.
(17) Pincus, P. *J. Chem. Phys.* **1981**, *75* (4), 1996–2000.
(18) Langer, J. S. *Acta Metall.* **1973**, *21*, 1649–1659.
(19) Langer, J. S. In *Solids Far From Equilibrium*; C., Godreche, Ed.; Cambridge University Press: New York, 1992.
(20) Olabisi, O.; Robeson, L. M.; Shaw, M. T. *Polymer–Polymer Miscibility*; Academic Press: New York, 1979; Chapter 2.